

# Beam test performance of a prototype muon trigger detector for the PSI muEDM experiment

Tianqi Hu<sup>1,2†</sup>, Jun Kai Ng<sup>1,2†</sup>, Guan Ming Wong<sup>1,2†</sup>, Cheng Chen<sup>1,2</sup>, Kim Siang Khaw<sup>1,2\*</sup>, Meng Lyu<sup>1,3</sup>, Angela Papa<sup>4,5,6</sup>, Philipp Schmidt-Wellenburg<sup>6</sup>, David Staeger<sup>6</sup>, Bastiano Vitali<sup>7,5</sup>

<sup>1</sup>Tsung-Dao Lee Institute, Shanghai Jiao Tong University, No.1 Lisuo Road, Shanghai, 201210, China.

<sup>2</sup>School of Physics and Astronomy, Shanghai Jiao Tong University, No.800 Dongchuan Road, Shanghai, 200240, China.

<sup>3</sup>School of Electronics, Information and Electrical Engineering, Shanghai Jiao Tong University, No.800 Dongchuan Road, Shanghai, 200240, China.

<sup>4</sup>Dipartimento di Fisica, Università di Pisa, Via B. Pontecorvo 3, Pisa, 56127, Italy.

<sup>5</sup>Sezione di Pisa, Istituto Nazionale di Fisica Nucleare, Largo B. Pontecorvo 3, Pisa, 56127, Italy.

<sup>6</sup>Laboratory for Particle Physics, Paul Scherrer Institut, Forschungsstrasse 111, Villigen PSI, 5232, Switzerland.

<sup>7</sup>Dipartimento di Fisica, Università di Roma “La Sapienza”, Piazzale Aldo Moro 2, Roma, 00815, Italy.

\*Corresponding author(s). E-mail(s): [kimsiang84@sjtu.edu.cn](mailto:kimsiang84@sjtu.edu.cn);

†These authors contributed equally to this work.

## Abstract

We report on the performance evaluation of a prototype muon trigger detector for the PSI muEDM experiment, conducted as a proof-of-principle test at the  $\pi$ E1 beamline of the Paul Scherrer Institute (PSI) using 27.5 MeV/c muons. The detector is designed to identify muons within the acceptance phase space of a compact storage solenoid and activate a pulsed magnetic kicker for muon storage; it was tested without the application of a magnetic field. It comprises a telescope made up of four scintillators in anticoincidence with a gate scintillator, all read out by silicon photomultipliers. The study focused on characterizing the detector’s response to various muon trajectories and the light yield of its plastic

scintillators. Experimental results demonstrated strong agreement with Geant4 Monte Carlo simulations that incorporate optical photon modeling, confirming the detector’s concept and its potential for meeting the stringent requirements of the muEDM experiment.

**Keywords:** trigger, electric dipole moment, silicon photomultiplier, optical photon

## 1 Introduction

The search for the muon electric dipole moment (EDM) represents one of the most promising avenues for probing physics beyond the Standard Model (SM). The current experimental limit on the muon EDM, set by the BNL E821 experiment [1],  $1.9 \times 10^{-19} e \cdot \text{cm}$ , is several orders of magnitude higher than the SM’s prediction [2–4]. By reaching an unprecedented sensitivity of  $6 \times 10^{-23} e \cdot \text{cm}$ , the PSI muEDM experiment [5–7] has the potential to reveal new physics, including hints of undiscovered particles or forces.

The significance of the lepton EDM searches stems from its potential to address key unresolved questions in modern physics, such as the baryon asymmetry of the universe [8, 9] via electroweak baryogenesis [10]. Despite the remarkable success of the SM in describing particle interactions, it fails to account for the observed matter-antimatter asymmetry, suggesting the existence of additional CP-violating sources beyond the SM. Detecting a non-zero EDM would provide direct evidence of such sources and offer insight into the mechanisms underlying this asymmetry.

The PSI muEDM experiment utilizes the innovative frozen-spin technique [11], where muons are stored in a compact solenoid with a radial electric field, canceling the muon  $g - 2$  anomalous spin precession. This setup minimizes disturbance from the much stronger magnetic moment and allows precise measurement of spin rotation due to a potential EDM. In the experiment, a surface muon beam is injected into a compact PSC solenoid through a narrow superconducting (SC) channel [12], as depicted in Fig. 1. Upon exiting the SC channel, the muon will be detected by a trigger detector [13]. For muon trajectories that match the storage phase space of the solenoid, a trigger signal will be generated by the detector. This trigger signal is used to activate a pulsed magnetic coil in the central region of the solenoid to deflect the trajectory of the muon into a stable orbit. Muons in the stable orbit will experience a radial E-field that cancels out the anomalous spin precession thus fulfilling the “frozen-spin” condition [14] of the experiment. The muon EDM measurement can then proceed by measuring the upstream-downstream asymmetry of the decay positron count versus time, caused by the muon spin precession out of the orbital plane due to the muon EDM.

In this work, we report on the performance of a prototype muon trigger detector, developed to meet the stringent requirements of the muEDM experiment. This detector features plastic scintillators read out by silicon photomultipliers (SiPMs) and is designed to balance high detection efficiency with minimal beam perturbation. A

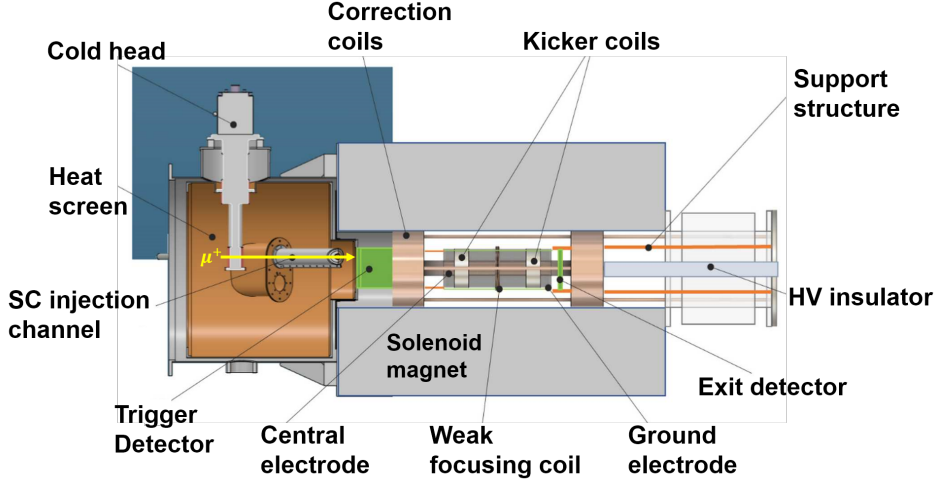


**Fig. 1** Overview of the muEDM experiment at PSI. Depicted is the Phase-I design of the experiment.

detailed beam test was conducted using the  $\pi$ E1 beamline at PSI with 27.5 MeV/c muons to evaluate the detector’s performance under various configurations.

This paper is structured as follows: Section 2 describes the design and operational principles of the muon trigger detector. Section 3 outlines the experimental setup, including the detector system, the data acquisition system, and the beamline configuration. Section 4 presents the results of beam profile measurements, event characterization, and decay positron studies. Section 5 validates these findings through Geant4-based simulations, and Section 6 concludes with a summary of the detector’s performance and its implications for the PSI muEDM experiment.

## 2 Muon trigger system

The muon trigger system [13] works in tandem with the magnetic pulse coil to store the muons for the muon EDM measurement. To maximize the sensitivity of the experiment, it must fulfill the following stringent requirements:

- Detection efficiency of the incoming muon must be as high as possible;
- Perturbations to the muon beam trajectories must remain minimal in order to maintain a high storage efficiency;
- Rejection rate of non-storable muons must be as high as possible so that the DAQ rate is reduced to a manageable level;
- The time delay between the incoming muon and the trigger pulse generation must be as minimal as possible.

After investigating various detection options, we have decided on detectors based on plastic scintillators read out by silicon photomultipliers as the design is more flexible, and fast readouts have been demonstrated in various experiments. To understand how such an upstream detection system would affect the muon EDM measurement, we

constructed a prototype muon trigger detector to address the top three requirements. The fourth requirement is addressed in a separate article using another version of the detector. The primary goal of the beam test was to measure the detector’s response to different muon trajectories in the simplest scenario (without magnetic field) and to obtain light yield information from the plastic scintillators.

The muon trigger detector system, as shown in Fig. 2, is composed of a gate detector and a telescope detector. If a muon passes through the gate detector without hitting the telescope sidewalls, it is potentially within the acceptance phase space and may be stored in a closed orbit. This means that in the case that both detectors observe a signal within the coincidence window, no trigger will be produced.

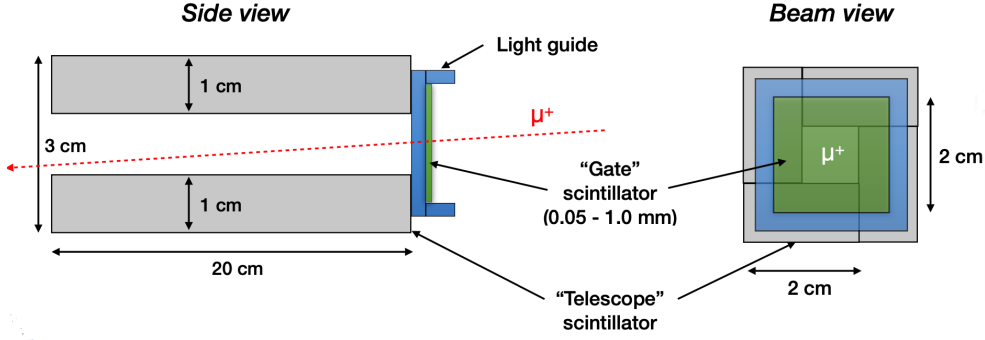


Fig. 2 A sketch of the prototype muon trigger detector.

The gate detector [15] is a 20 mm × 20 mm × 0.1 mm scintillator tile with an optical frame of 2 mm × 2 mm cross section attached to the outer edge to which the NDL EQR15-6060 SiPMs are attached. The thickness was chosen based on a simulation study to balance between multiple scattering and light yield in the scintillator.

The telescope detector is composed of four GNKD HND-S2 scintillator bars, with the size of 20 mm × 10 mm × 200 mm. These scintillators are inserted into a rectangular, compact, and symmetrical 3D printed holder. Photons produced in one scintillator bar would be also transmitted to other scintillator bars through optical cross-talk. The NDL silicon photomultiplier (SiPM)<sup>1</sup> with an active area 6 mm × 6 mm was optically coupled to the downstream end of each plastic scintillator using BC-630 optical grease.

### 3 Beam test configuration

#### 3.1 Beam configuration

The beam test measurements and analysis described herein are based on a two-week run using the  $\pi$ E1 beamline at PSI in Nov-Dec 2022. The beamline was tuned to transport muons at a momentum of 27.5 MeV/c. A scintillator-based beam counter on a 3-axis movable platform was setup in the downstream. The downstream beamline

<sup>1</sup>developed by the Novel Device Laboratory: <http://www.ndl-sipm.net>

optics were tuned to maximize the count rate, with the counter positioned at  $z = 0$  mm (roughly 300 mm from the last quadrupole of the  $\pi E1$  beamline) and  $z = 246$  mm respectively. All tests described in the following were performed using the 27.5 MeV/c muon beam at the  $\pi E1$  beamline of PSI. There are two different beam settings tuned by quadrupole focusing of the  $\pi E1$  beamline: Beam Tune A, which focuses the muon beam close to the gate detector ( $z = 0$  mm), and Beam Tune B, which focuses the muon beam close to the exit detector ( $z = 246$  mm).

### 3.2 Experimental setup

Prior to the performance measurement of the prototype muon trigger detector, several detectors were installed and used to measure the muon beam profile:

- **Veto detector:** A scintillator tile, size 80 mm  $\times$  80 mm  $\times$  5 mm, with a hole of diameter 18 mm at the center. This detector serves as a selection aperture matching approximately the geometrical acceptance of the telescope. Only muons going through the hole are taken into account.
- **Exit detector:** Behind the telescope detector, a thick scintillating tile size 80 mm  $\times$  80 mm  $\times$  5 mm is used as the exit trigger of the setup.
- **Beam profile scanner:** Downstream of the entire setup, a 2D beam profile monitor (SiMon) was installed to measure the exit muon beam profile and quantify muons outside the geometrical acceptance of the prototype muon trigger detector.

The experimental setup during the test beam is shown in Fig. 3. These auxiliary detectors ensured precise alignment and provided detailed measurements of the beam profile, helping to quantify the muon trajectories and evaluate the system's performance.

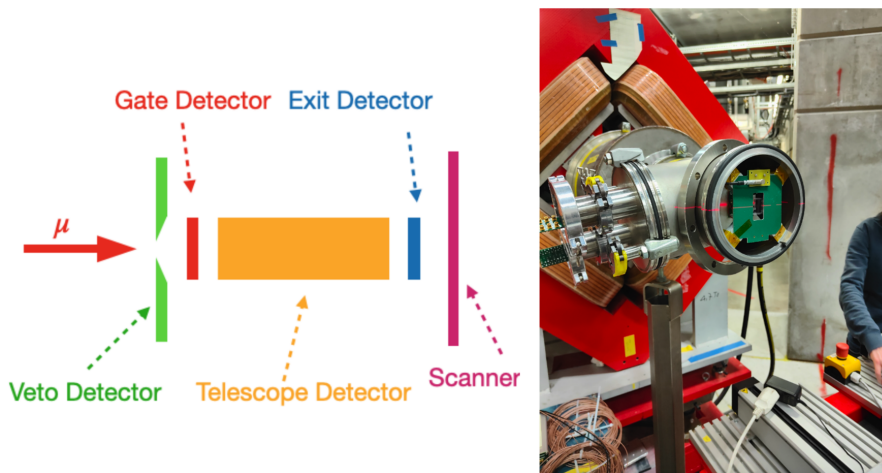


**Fig. 3** Left: schematics of modified telescope detector; right: prototype muon trigger detector installed in the vacuum tube and aligned with laser.

A fully constructed muon trigger detector is shown in Fig. 4. The setup was then installed in a vacuum flange to minimize the muon scattering with the air during the beam test.

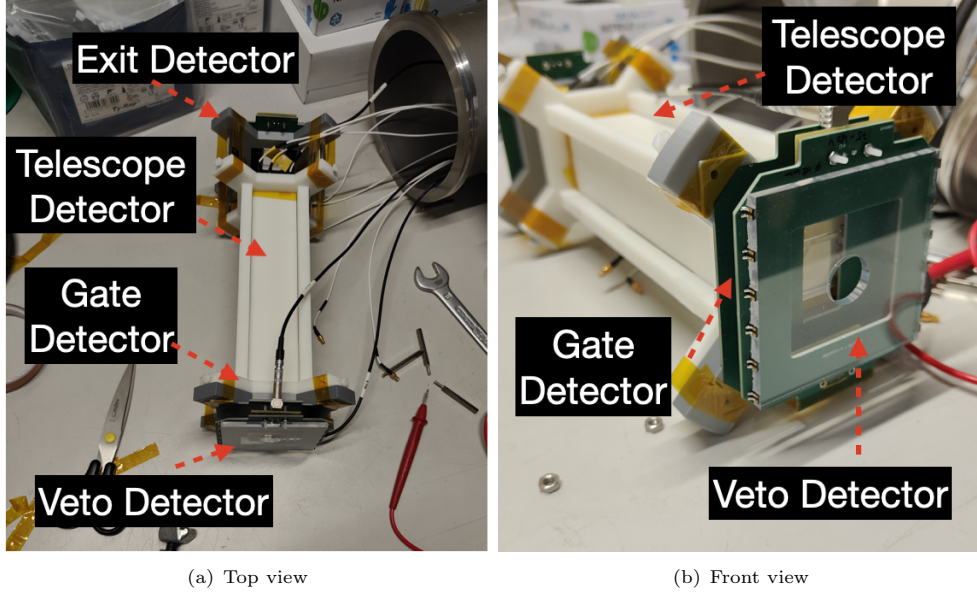


**Fig. 4** (a) Top and (b) front view of the muon trigger detector during the beam test at PSI.

### 3.3 Data Acquisition

The Data Acquisition System (DAQ) employed in this experiment was the Wave-Dream Board (WDB) [16], a 16-channel system developed at PSI for the MEG II experiment. The WDB integrates an advanced power supply and amplifier, allowing it to handle high-speed, high-precision signals essential for particle physics experiments. Its compact design and multi-channel capability make it well-suited for managing the complex data requirements of the prototype muon trigger detector.

Figure 5 illustrates a screenshot from the WDB software, highlighting the signals captured during the beam test. The positive signals correspond to the four NDLSiPMS attached to the telescope detector, while the negative signals represent the veto detector, gate detector, and exit detector channels. The top right corner of Fig. 5 displays detailed information about each channel's trigger levels and gain settings, enabling precise control and optimization of the DAQ system.

During the beam test, approximately 0.7 million events were recorded under various trigger configurations as summarized in Tab. 1. These triggers were designed to capture a comprehensive range of muon trajectories and interactions within the detector system. The configurations included:

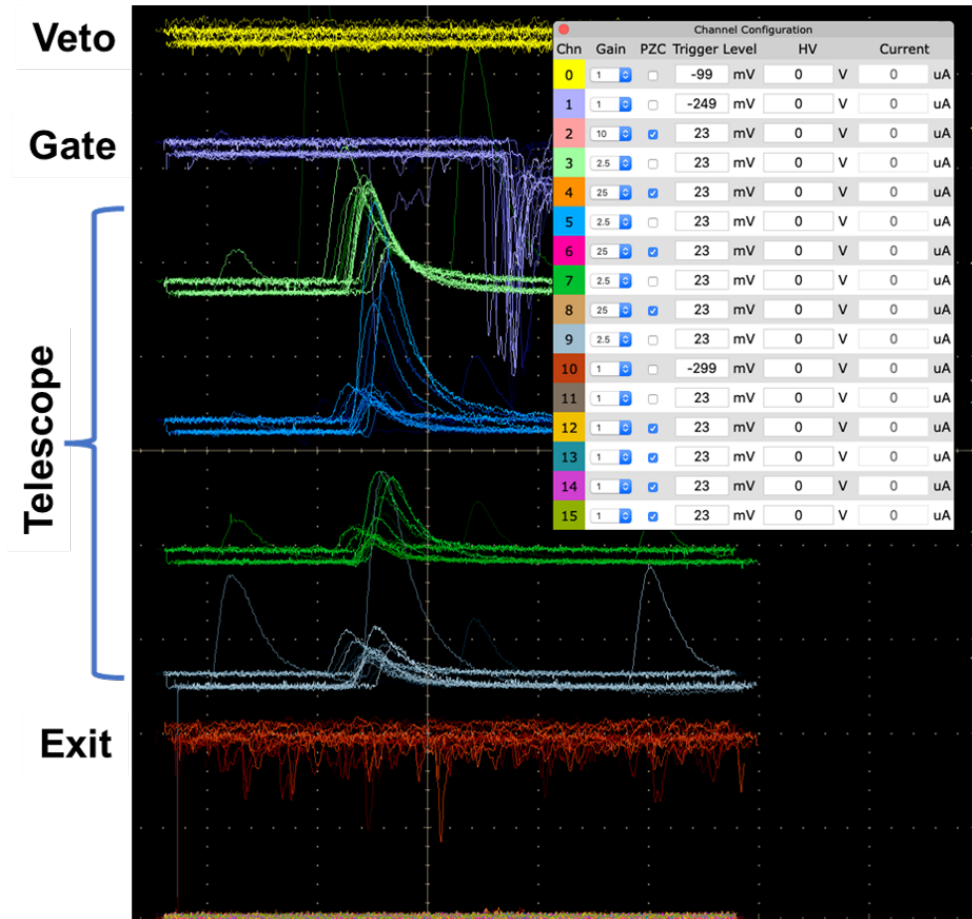


Fig. 5 The observed signals at the Wave Dream Board monitor.

1. **Gate Self-Trigger:** Events were recorded when a muon hit the gate detector, independent of signals from other detectors.
2. **Gate and Exit Coincidence:** Events were captured only when signals were registered simultaneously in both the gate and exit detectors, isolating muons that traversed the detector system
3. **Gate and Telescope Coincidence:** This setting recorded events where signals were simultaneously detected in the gate and telescope detectors, focusing on interactions within the telescope

The DAQ system's high sampling rate and low noise level ensured accurate signal capture and timing resolution, critical for differentiating between primary muon events and decay positrons. Its robust design also allowed seamless integration with the prototype detector setup, enabling efficient data collection during the two-week beam test.

**Table 1** Collected datasets during the beam test.

Trigger Model	Statistics	
	Beam Tune A	Beam Tune B
Gate Self-Trigger	100,000	150,000
Gate and Exit	100,000	150,000
Gate and Telescope	100,000	100,000

## 4 Experimental results

### 4.1 Beam profile extraction

The beam profile measurements were crucial for understanding the spatial distribution and focusing properties of the 27.5 MeV/c muon beam at the  $\pi$ E1 beamline. These measurements informed the alignment and optimization of the prototype detector and facilitated the characterization of muon trajectories within the experimental setup.

Beam profiles were acquired using a combination of auxiliary detectors, including a veto detector with a central aperture, an exit detector, and a 2D beam profile monitor (SiMon) positioned downstream. The veto detector ensured that only muons within the expected acceptance region were considered for further analysis. The SiMon monitor provided high-resolution measurements of the transverse beam distribution at multiple positions along the beamline.

Figures 6 and 7 illustrate the beam profiles for both tunes, measured at  $z = 0$  mm and  $z = 246$  mm, respectively. The profiles showed clear variations in beam size and intensity distribution, reflecting the effect of the quadrupole tuning parameters. For Beam Tune A, the beam was more collimated at  $z = 0$  mm, whereas Beam Tune B produced a broader distribution at the same position.

The beam sizes at different positions along the beamline were determined by fitting the measured profiles to Gaussian distributions. These sizes were corrected for Coulomb scattering effects in air to ensure accuracy. Using the corrected beam sizes, the beam optics formalism was applied to extract the Twiss parameters, including the horizontal and vertical beta functions and the emittance. These parameters provided a comprehensive description of the beam’s phase space and were consistent with the expected beamline configuration.

Precise alignment of the detector components was achieved by cross-referencing the beam profiles with the known geometry of the setup. The alignment ensured that the beam trajectory intersected critical detector regions, such as the central aperture of the veto detector and the telescope scintillators. The measured profiles were also used as input for Geant4-based simulations, allowing direct comparison between measured and simulated beam distributions. As shown in Fig. 12, the simulated phase space of the beam closely matched the experimental data, validating the accuracy of the beam model and the alignment procedure.

### 4.2 Event characteristics and distributions

To characterize the response of the prototype muon trigger detector, we analyzed the distribution of event topologies under different trigger models and beam tunes



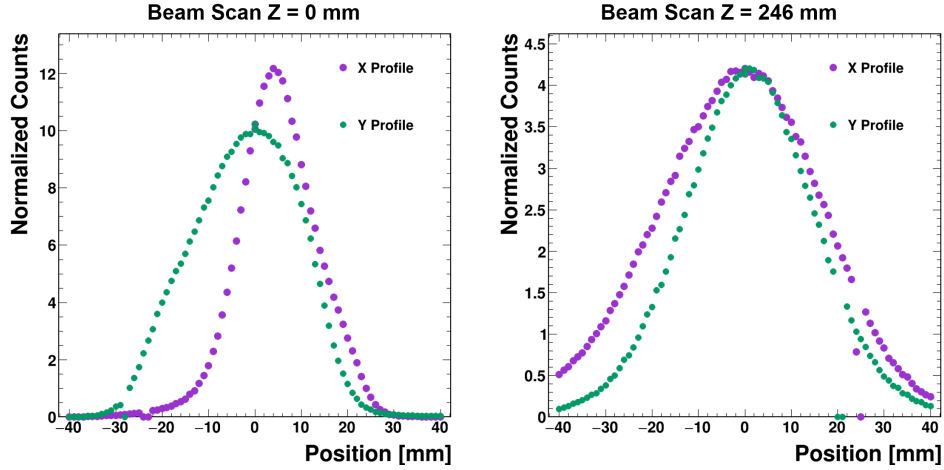


Fig. 6 Beam Tune A profile measurement, beam focused at  $z = 0$  mm. Left: profile measured at  $z = 0$  mm; right: measured at  $z = 246$  mm.

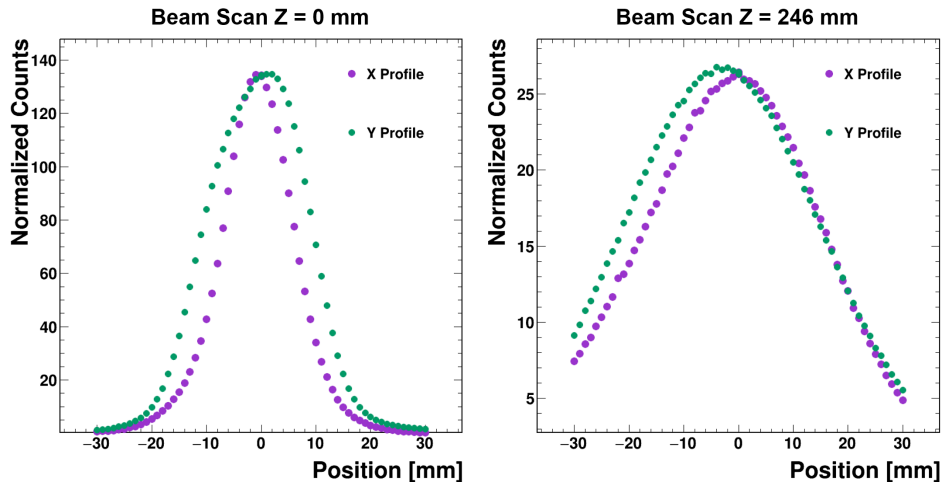


Fig. 7 Beam Tune B profile measurement, beam focused at  $z = 246$  mm. Left: profile measured at  $z = 0$  mm; right: measured at  $z = 246$  mm.

for the dataset collected during the beam test. The SiPM threshold was set to 4.5 photoelectrons (p.e.), effectively suppressing dark noise while reliably selecting muon events detected by the telescope. This threshold was applied uniformly during online data acquisition and offline analysis.

Event classification was performed based on the combination of signals from the veto, gate, telescope, and exit detectors. These configurations helped distinguish between muons that passed through the acceptance region, stopped in the telescope, or scattered outside the defined geometry. Table 2 summarizes the measured event distributions for each trigger model, with representative topologies visualized in Fig. 8.

For instance, the topology “(!Veto) & Telescope & (!Exit)” corresponds to events where the muon bypassed the veto detector (indicating passage through the central hole), produced a signal in the telescope detector, but did not reach the exit detector. Such events typically arise from muons stopping within the telescope or scattering outside the exit detector’s acceptance.

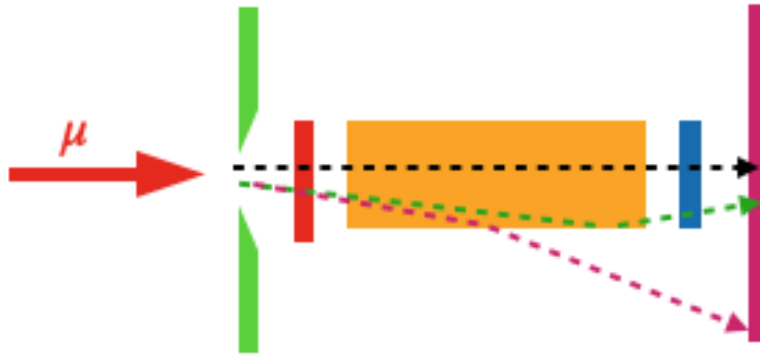
We observed distinct event distributions for the three trigger models:

- **Gate Self-Trigger:** This model recorded a higher proportion of events where muons interacted with the telescope but did not reach the exit detector. These results align with the expectation that some muons are stopped or scattered by the telescope scintillators.
- **Gate and Exit Coincidence:** Events under this model predominantly included muons traversing the full acceptance region and triggering both detectors. The proportion of such events was consistent with the geometric acceptance and beam focusing parameters.
- **Gate and Telescope Coincidence:** This configuration effectively isolated interactions within the telescope detector, providing critical data on muon scattering and photon collection efficiency.

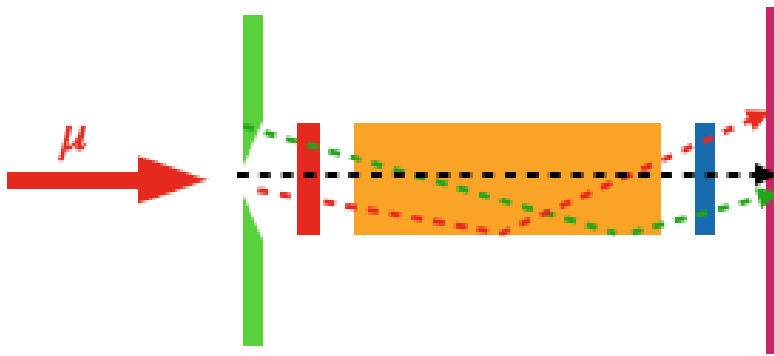
**Table 2** Measured distribution for each trigger mode and event topology. In the table, “!” represents that no signal was recorded in the specified detectors, for example ‘!Veto’ represents that no signal was registered in the veto detector, and “&” represents a coincidence between two readouts.

Trigger Mode	Event Topology	Beam Tune A	Beam Tune B
Gate Self-Trigger	(!Veto) & Telescope & (!Exit)	86.72%	83.99%
	(!Veto) & Telescope & Exit	0.75%	1.17%
	(!Veto) & (!Telescope) & Exit	2.78%	4.78%
Gate and Exit	Veto	4.47%	4.86%
	(!Veto) & Telescope	19.53%	18.34%
	(!Veto) & !Telescope	76.00%	76.80%
Gate and Telescope	(!Veto) & (!Exit)	87.71%	84.65%
	(!Veto) & Exit	3.59%	5.77%

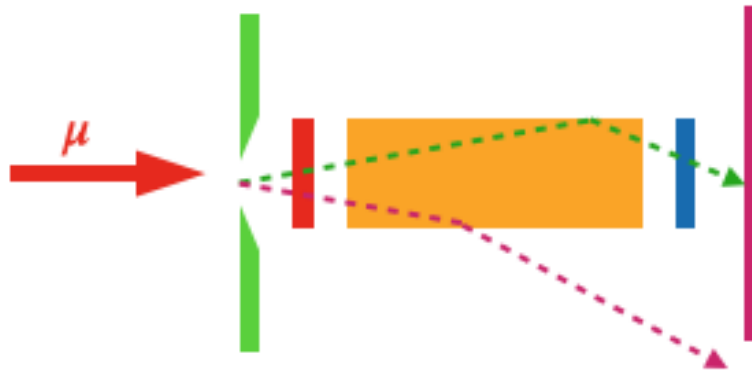
The spatial distribution of events revealed beam trajectory variations and their impact on muon interactions. Events were more concentrated near the central region under Beam Tune A, while Beam Tune B produced a broader distribution near the exit detector. These observations were consistent with the measured beam profiles (Fig. 6 and 7) and provided additional insight into beam alignment and focusing effects.



(a) Gate detector self-trigger



(b) Gate coincide with Exit



(c) Gate coincide with Telescope

**Fig. 8** Event topology for different trigger modes (For the details of detectors, refer Fig. 3 (Left))

### 4.3 Decay positron signals

During offline waveform reconstruction, two distinct peaks were identified in some events, as shown in Fig. 9. Given the muon momentum of  $27.5 \text{ MeV}/c$ , it is expected that muons would stop within the telescope detector scintillator, allowing their decay positron signals to be observed. To confirm the origin of the later peak as arising from a decay positron, we analyzed the time intervals ( $\Delta T$ ) between the two peaks.

The distribution of  $\Delta T$  was fitted with the exponential decay function  $N_0 e^{-\Delta T/\tau}$ , where  $N_0$  is the normalization, and  $\tau$  the muon lifetime. The results for one of the scintillators in the telescope detector are shown in Fig. 9(b). The fitted exponential decay constant yielded a lifetime of  $2.15(19) \mu s$ , which is in good agreement with the established muon lifetime of  $2.197 \mu s$  [17]. Despite the large uncertainty, the analysis validates the detector’s capability to capture and resolve decay positron signals with high temporal accuracy.

### 4.4 Photon statistics

The photon statistics measured during the beam test provided valuable insights into the optical performance of the prototype detector. This analysis is critical for evaluating the scintillator light yield, the SiPM response, and the effectiveness of the detector in capturing and analyzing muon interactions.

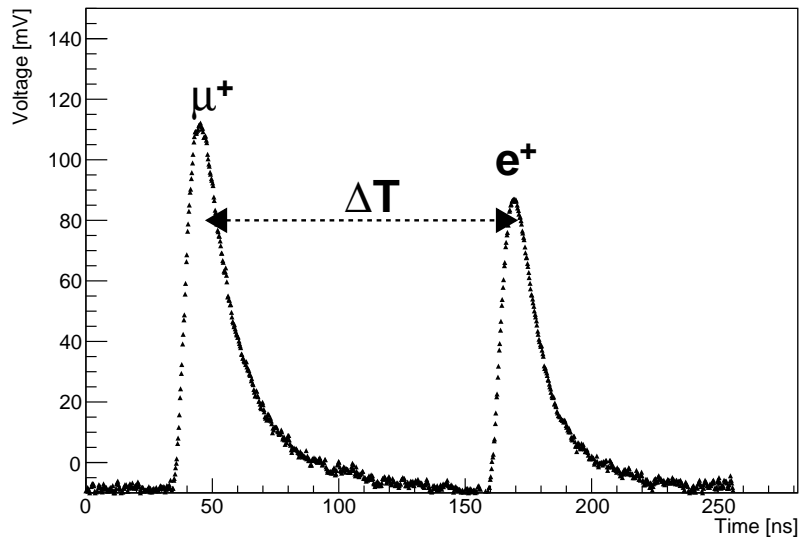
The telescope detector consisted of four scintillator bars as shown in Fig. 10, each coupled to a silicon photomultiplier (SiPM). When a muon traversed the scintillator, it generated photons via scintillation, which were subsequently collected by the SiPM attached to the corresponding bar. Optical cross-talk between adjacent scintillators also resulted in photon collection by neighboring SiPMs.

On average, more than 300 photons per muon event were collected by the SiPM attached to the scintillator directly hit by the muon. Adjacent scintillators collected between 100 and 120 photons, while the opposite scintillator registered approximately 50 photons. These measurements are consistent with expectations based on the optical properties of the scintillator and the geometry of the setup. The observed photon yields were sufficient to generate robust anti-coincidence signals, a key requirement for the detector’s performance.

Photon distributions were analyzed to assess the symmetry and cross-talk effects between the scintillators. Correlation plots, such as those for adjacent and opposite scintillators, revealed characteristic patterns of photon sharing. For instance, the correlation between the top and adjacent SiPMs exhibited multiple peaks, reflecting the expected distribution of photons due to optical cross-talk. Similarly, the correlation between the top and opposite SiPMs displayed a single, lower-intensity peak, consistent with minimal cross-talk. Figures 11(c) and 11(d) illustrate these correlations, showing strong agreement between experimental data and theoretical expectations.

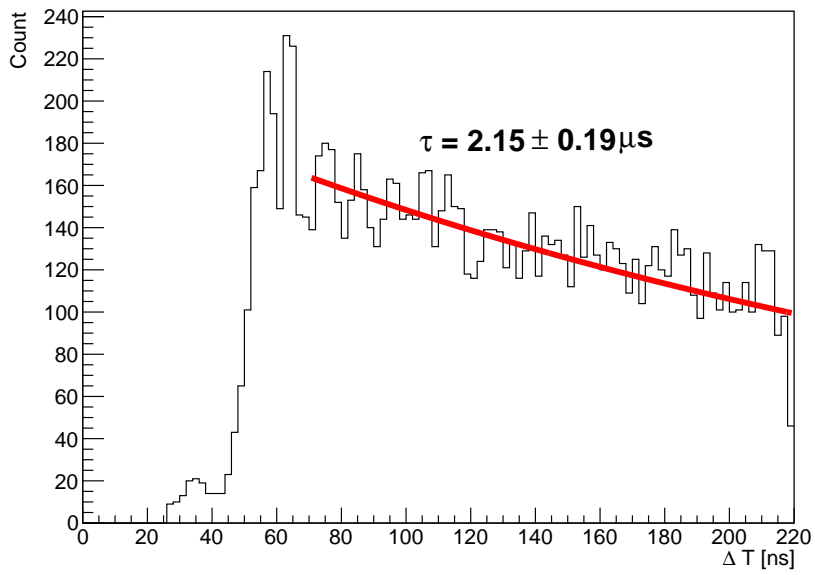
Time-resolved analysis of the photon signals was conducted to evaluate the temporal behavior of the detector. The SiPMs demonstrated prompt response times, ensuring accurate timing information for muon and decay positron events. This characteristic is particularly important for distinguishing overlapping events and minimizing background noise. A time cut of 250 ns, matching the time window of the Wave Dream

### The Muon and Positron Signal



(a) Two peaks shown in one event

### $\Delta T$ distribution



(b) Time interval distribution

**Fig. 9** Decayed Positron Signal.

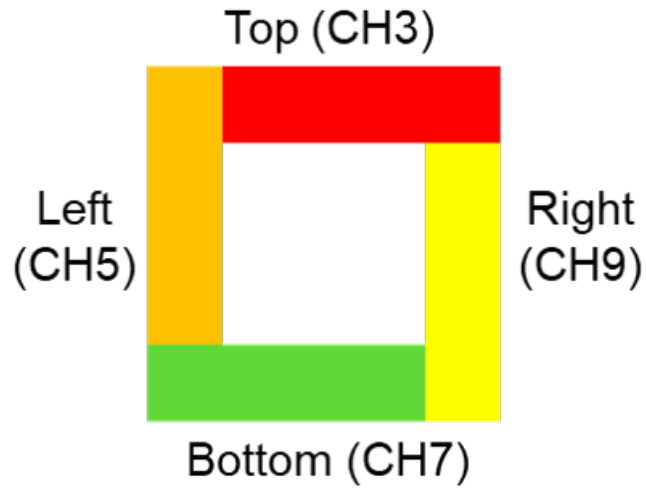
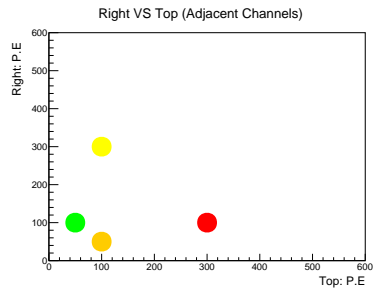
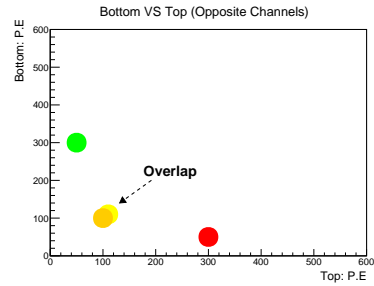


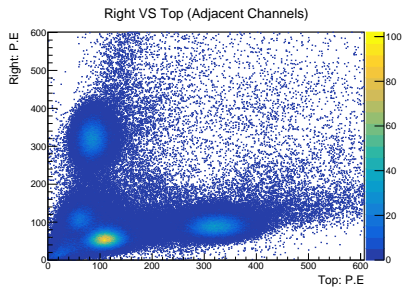
**Fig. 10** Layout of the telescope channel arrangement



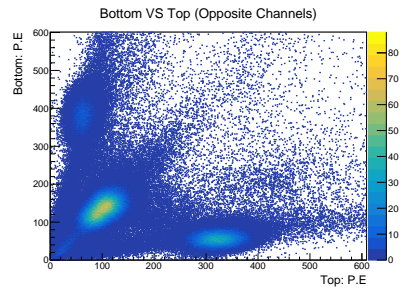
(a) Expected optical photon number correlation of adjacent channels (CH9 vs CH3)



(b) Expected correlation of opposite channels (CH7 vs CH3)



(c) Measured optical photon number correlation of adjacent channels (CH9 vs CH3)



(d) Measured optical photon number correlation of opposite channels (CH7 vs CH3)

**Fig. 11** Correlation plot of photon distribution for each pair of scintillators in the telescope detector.

Board (WDB), was applied during data processing to focus on relevant signals while suppressing noise.

The measured photon statistics were validated using Geant4-based simulations, which incorporated detailed optical models of the scintillator materials and the SiPM photon detection efficiency (PDE). Simulated distributions closely matched the experimental results, reproducing both the absolute photon yields and the correlation patterns observed in the data. This agreement underscores the accuracy of the detector design and its optical modeling, providing confidence in its performance during future experiments.

## 5 Simulation Verification

To validate the performance of the prototype muon trigger detector, a comprehensive set of Monte Carlo simulations was conducted using a Geant4-based framework, *musr-Sim* [18]. These simulations were designed to reproduce the experimental conditions, including beam dynamics, detector geometry, and optical photon propagation. The simulation results were compared to the experimental data to evaluate the detector's response and confirm its design accuracy.

The analysis focused on two key aspects:

- **Beam Distribution:** Simulating the muon beam's phase space and trajectory to ensure consistency with measured profiles and Twiss parameters.
- **Optical Photon Distribution:** Reproducing the light yield and photon sharing among the scintillators, accounting for cross-talk and SiPM efficiency.

The agreement between the simulated and experimental data demonstrated a robust understanding of the detector's behavior, reinforcing confidence in its design and its suitability for the stringent requirements of the muEDM experiment.

### 5.1 Beam distribution

Measured beam profiles of the test beam are used as input for the simulation beam model. First we fitted for the Twiss parameters of the beam using the measured beam horizontal and vertical profiles. Then we use the fitted Twiss parameters to generate muon events in the simulation. As shown in Fig. 12, the phase space of the generated muon are in good agreement with the measurement. The agreement between measured and simulated beam sizes can also be seen in and the generated muon are in good agreement with the measurement.

The events are characterized at the truth level and subsequently at a higher level with optical photons. Beam tune effects on the detector are also studied at the truth level. Truth-level studies involved event characterization for events where hits are deposited in respective sub-detectors. At the truth level, the relative event rates agree in trend with the measured result. Alterations in the beam tunes depicted minimal impact on the event rates.

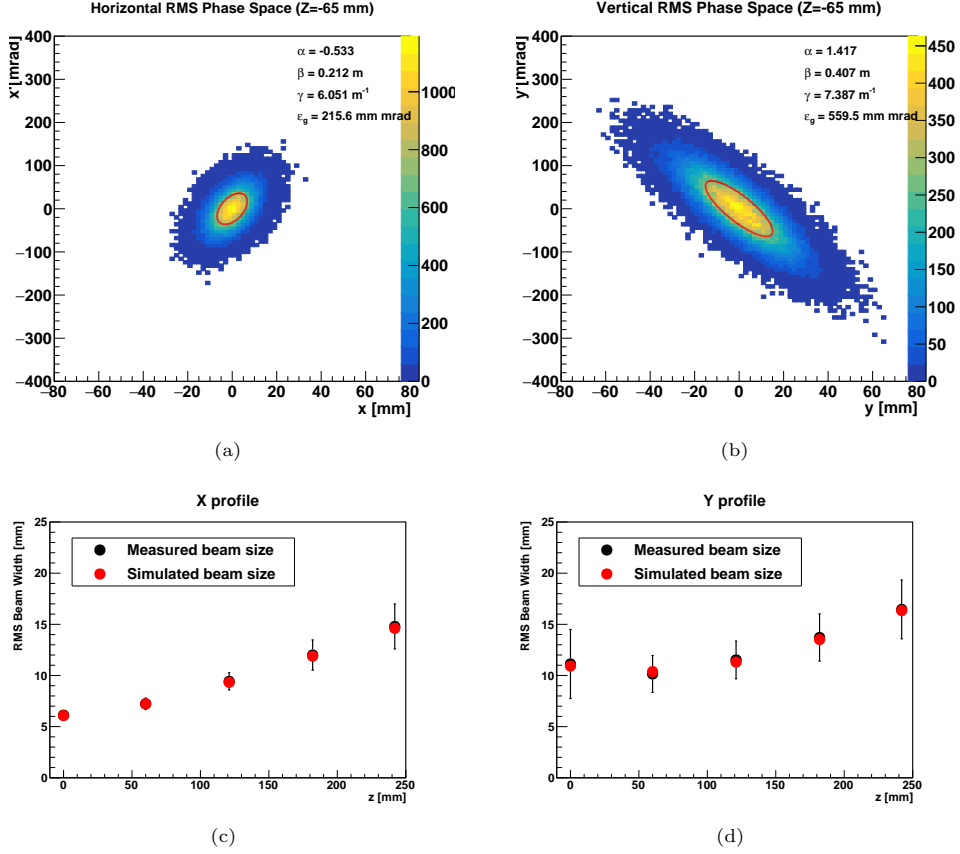


**Fig. 12** Top: Beam phase space of test beam reproduced in simulation, the red profile is the elliptical function obtained from measured Twiss parameters; bottom: X and Y profiles of measured beam sizes reproduced in simulation.

## 5.2 Optical photon distribution

The distribution of optical photons is initially reproduced to comprehend the optical characteristics of the telescope scintillators, particularly the optical transmittance between each scintillator. Key parameters that may exert a substantial influence on the optical characteristics are identified. These parameters can be classified into material and surface properties [19].

Data sheet values of scintillators are used as input for material properties, of which the *scintillation yield* and *scintillation spectrum* result in the most notable changes. The photon detection efficiency (PDE) spectrum of the SiPM is implemented for the surface boundaries between the telescopes and SiPM.

With these inputs and fine-tunes, along with a time-cut ( $t_{cut} \leq 250$  ns) added for the simulated optical photons, which corresponds to the time-window of WDB, the optical photon distribution is closely reproduced (Fig. 13).



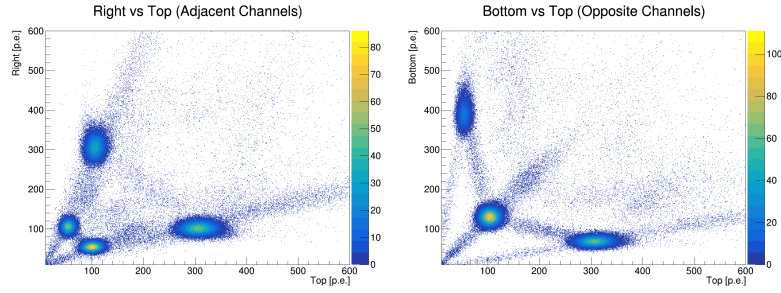


**Fig. 13** Optical photon distribution reproduced in simulation, having a good agreement with Fig. 11(c) and Fig. 11(d).

The relative event rates are reproduced using optical photon distribution with the implemented optical characteristics that closely signify the measured results (Fig. 14). Event characterization by optical photon signals has a noticeable improvement from that of truth hits. Both the truth and optical simulation agree in trend where the beam focuses have minimal effect on the event rates. The optical simulation however better reproduces the rates at which the trigger is of both gate and exit detectors, where ideal events have a significant increase.

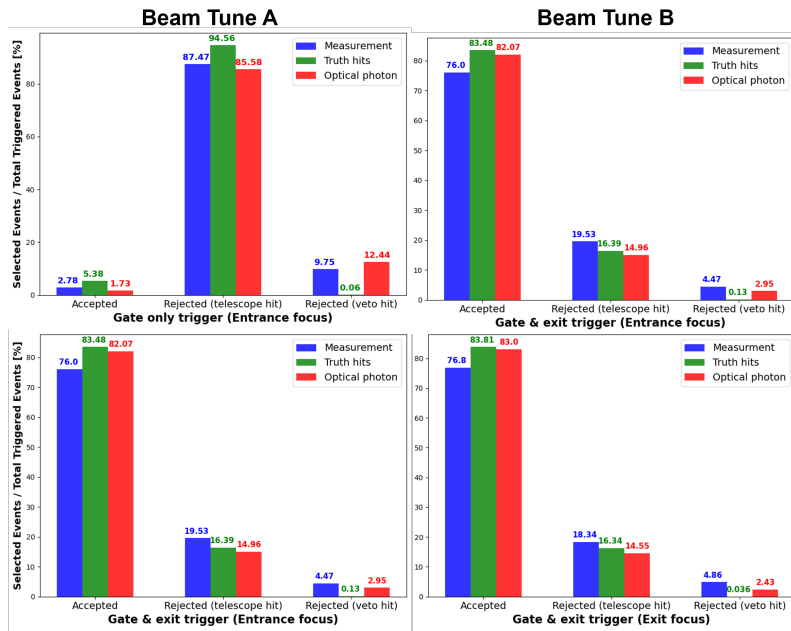


**Fig. 14** Comparing event rates of measurement with simulation using truth hits and optical photons.

## 6 Conclusion

A prototype telescope detector for the muEDM experiment was successfully constructed using four GNKD HND-S2 scintillator bars and NDL EQR15-6060 SiPMs, and it was tested at the PSI  $\pi$ E1 beamline with a 27.5 MeV/ $c$  muon beam. The event rates were measured under three distinct trigger models, revealing that approximately 2–5% of the beam muons pass through the gate detector without interacting with the telescope. For muons on the correct trajectory (i.e., passing through both the gate and exit detectors), the triggering efficiency was measured at 75%.

Double signals were observed, corresponding to muons decaying into positrons within one of the scintillators. These events were confirmed by the characteristic time distribution between the two signals. Photon collection by the SiPMs was consistent with expectations, with more than 300 photons detected by the SiPM attached to the hit scintillator and 50–120 photons recorded by other SiPMs, sufficient to produce the anti-coincidence signal.

The results were cross-validated using Geant4-based simulations, which showed good agreement with the measured event rates at the optical photon level. This agreement demonstrates a robust understanding of the prototype detector's response, providing a solid foundation for further development and commissioning of the muEDM experimental setup.

**Acknowledgments.** The project is supported by the Science Foundation of China under Grant 12050410233 and the China Scholarship Council No. 202206230093. Additionally, this work is partially funded by the Swiss National Science Fund through grants 204118 and 220487 and receives financial support from the Swiss State Secretariat for Education, Research, and Innovation (SERI) under grant number MB22.00040. We wish to express our sincere gratitude to A. Soter and D. Göldi for their efforts in ensuring the SiMon detector was adequately prepared prior to our designated beam time. Furthermore, we acknowledge the significant assistance provided by A. Knecht and A. Antognini before and during our test beam times on the  $\pi$ E1 beam line.

## References

- [1] Bennett, G.W., *et al.*: An Improved Limit on the Muon Electric Dipole Moment. Phys. Rev. D **80**, 052008 (2009) <https://doi.org/10.1103/PhysRevD.80.052008> [arXiv:0811.1207](https://arxiv.org/abs/0811.1207) [hep-ex]
- [2] Pospelov, M., Ritz, A.: CKM benchmarks for electron electric dipole moment experiments. Phys. Rev. D **89**(5), 056006 (2014) <https://doi.org/10.1103/PhysRevD.89.056006> [arXiv:1311.5537](https://arxiv.org/abs/1311.5537) [hep-ph]
- [3] Ghosh, D., Sato, R.: Lepton Electric Dipole Moment and Strong CP Violation. Phys. Lett. B **777**, 335–339 (2018) <https://doi.org/10.1016/j.physletb.2017.12.052> [arXiv:1709.05866](https://arxiv.org/abs/1709.05866) [hep-ph]

- [4] Yamaguchi, Y., Yamanaka, N.: Large long-distance contributions to the electric dipole moments of charged leptons in the standard model. *Phys. Rev. Lett.* **125**, 241802 (2020) <https://doi.org/10.1103/PhysRevLett.125.241802> [arXiv:2003.08195](https://arxiv.org/abs/2003.08195) [hep-ph]
- [5] Adelman, A., et al.: Search for a muon EDM using the frozen-spin technique (2021) [arXiv:2102.08838](https://arxiv.org/abs/2102.08838) [hep-ex]
- [6] Cavoto, G., *et al.*: Anomalous spin precession systematic effects in the search for a muon EDM using the frozen-spin technique. *Eur. Phys. J. C* **84**(3), 262 (2024) <https://doi.org/10.1140/epjc/s10052-024-12604-0> [arXiv:2311.10508](https://arxiv.org/abs/2311.10508) [hep-ex]
- [7] Khaw, K.S., Chen, C., Giovannozzi, M., Hu, T., Lv, M., Ng, J.K., Papa, A., Schmidt-Wellenburg, P., Vitali, B., Wong, G.M.: Status of the muEDM Experiment at PSI †. *Phys. Sci. Forum* **8**(1), 50 (2023) <https://doi.org/10.3390/psf2023008050> [arXiv:2307.01535](https://arxiv.org/abs/2307.01535) [hep-ex]
- [8] Sakharov, A.D.: Violation of CP Invariance, C asymmetry, and baryon asymmetry of the universe. *Pisma Zh. Eksp. Teor. Fiz.* **5**, 32–35 (1967) <https://doi.org/10.1070/PU1991v034n05ABEH002497>
- [9] Komatsu, E., *et al.*: Seven-Year Wilkinson Microwave Anisotropy Probe (WMAP) Observations: Cosmological Interpretation. *Astrophys. J. Suppl.* **192**, 18 (2011) <https://doi.org/10.1088/0067-0049/192/2/18> [arXiv:1001.4538](https://arxiv.org/abs/1001.4538) [astro-ph.CO]
- [10] Morrissey, D.E., Ramsey-Musolf, M.J.: Electroweak baryogenesis. *New J. Phys.* **14**, 125003 (2012) <https://doi.org/10.1088/1367-2630/14/12/125003> [arXiv:1206.2942](https://arxiv.org/abs/1206.2942) [hep-ph]
- [11] Farley, F.J.M., Jungmann, K., Miller, J.P., Morse, W.M., Orlov, Y.F., Roberts, B.L., Semertzidis, Y.K., Silenko, A., Stephenson, E.J.: A New method of measuring electric dipole moments in storage rings. *Phys. Rev. Lett.* **93**, 052001 (2004) <https://doi.org/10.1103/PhysRevLett.93.052001> [arXiv:hep-ex/0307006](https://arxiv.org/abs/hep-ex/0307006)
- [12] Doinaki, A., *et al.*: Superconducting shield for the injection channel of the muEDM experiment at PSI. *JINST* **18**(10), 10011 (2023) <https://doi.org/10.1088/1748-0221/18/10/C10011>
- [13] Wong, G.M., Ng, J.K., Hu, T., Lyu, M., Khaw, K.S.: Research and development of a muon entrance trigger for the muEDM experiment at PSI. *Nucl. Part. Phys. Proc.* **346**, 58–62 (2024) <https://doi.org/10.1016/j.nuclphysbps.2024.05.014>
- [14] Hume, T., Chakraborty, R., Doinaki, A., Dutsov, C., Giovannozzi, M., Michielsen, K., Morvaj, L., Papa, A., Schmidt-Wellenburg, P., Stäger, D.: Implementation of the frozen-spin technique for the search for a muon electric dipole moment. *JINST* **19**(01), 01021 (2024) <https://doi.org/10.1088/1748-0221/19/01/P01021>

- [15] Stäger, D.: Measurement of the detection efficiency of a 100  $\mu\text{m}$  thin plastic scintillator for muons with  $p = 28 \text{ MeV}/c$ . JINST **18**(11), 11029 (2023) <https://doi.org/10.1088/1748-0221/18/11/C11029>
- [16] Galli, L., *et al.*: WaveDAQ: An highly integrated trigger and data acquisition system. Nucl. Instrum. Meth. A **936**, 399–400 (2019) <https://doi.org/10.1016/j.nima.2018.07.067>
- [17] Tishchenko, V., *et al.*: Detailed Report of the MuLan Measurement of the Positive Muon Lifetime and Determination of the Fermi Constant. Phys. Rev. D **87**(5), 052003 (2013) <https://doi.org/10.1103/PhysRevD.87.052003> [arXiv:1211.0960](https://arxiv.org/abs/1211.0960) [hep-ex]
- [18] Sedlak, K., Scheuermann, R., Shiroka, T., Stoykov, A., Raselli, A.R., Amato, A.: Musrsim and musrsimana - simulation tools for  $\mu\text{sr}$  instruments. Physics Procedia **30**, 61–64 (2012) <https://doi.org/10.1016/j.phpro.2012.04.040> . 12th International Conference on Muon Spin Rotation, Relaxation and Resonance ( $\mu\text{SR}2011$ )
- [19] Nilsson, J., Cuplov, V., Isaksson, M.: Identifying key surface parameters for optical photon transport in geant4/gate simulations. Applied Radiation and Isotopes **103**, 15–24 (2015) <https://doi.org/10.1016/j.apradiso.2015.04.017>